

Incompressibility and density distributions in asymmetric nuclear systems

S. Yoshida,¹ H. Sagawa,² and N. Takigawa³

¹*Department of Physics, Hosei University, Fujimi, Chiyoda, Tokyo 102-8160, Japan*

²*Center for Mathematical Sciences, University of Aizu, Ikki-machi, Aizu-Wakamatsu, Fukushima 965, Japan*

³*Department of Physics, Graduate School of Science, Tohoku University, Sendai 980-8578, Japan*

(Received 5 June 1998)

The incompressibility of asymmetric nuclear matter K_∞ is studied analytically within the framework of the relativistic mean field theory and the nonrelativistic Skyrme Hartree-Fock model. We investigate also the relation between K_∞ of asymmetric nuclear matter and the surface diffuseness by using the extended Thomas Fermi approximation. The self-consistent relativistic and nonrelativistic mean field calculations are performed for Sn isotopes, taking into account the pairing correlation, in order to extract the asymmetry parameter $(N - Z)/A$ dependences of the surface diffuseness a and the central density $\rho(r=0)$. Clear correlations are found between the incompressibility K_∞ of asymmetric nuclear matter and the extracted surface diffuseness a , and also between K_∞ and the extracted central density $\rho(r=0)$. [S0556-2813(98)03511-0]

PACS number(s): 21.10.Ft, 21.10.Gv, 21.60.-n, 21.65.+f

I. INTRODUCTION

The incompressibility K_∞ of nuclear matter is one of the most important ingredients for the nuclear equation of state (EOS), which influences both ground and excited state properties of nuclei, fragmentations of heavy ion collisions and several astrophysical phenomena, for example, supernova explosion. The incompressibility K_∞ of nuclear matter is defined by the second derivative of the energy density per nucleon with respect to the density at the saturation point of nuclear matter,

$$K_\infty = 9 \left[\rho^2 \frac{\partial^2}{\partial \rho^2} \left(\frac{\mathcal{H}}{\rho} \right) \right]_{\rho=\rho_0}, \quad (1)$$

where ρ_0 is the saturation density and \mathcal{H} is the energy density of nuclear matter. Effective nuclear forces used in both nonrelativistic and relativistic mean field calculations are demanded to reproduce empirical values of the binding energy and the density at the saturation point of nuclear matter. It has been known that the incompressibility is ill-determined showing a large variety among the adopted interactions, although the mean field calculations reproduce reasonably well the binding energies and the rms radii of many nuclei in a wide range of mass table. The nuclear breathing mode, namely isoscalar giant monopole resonance (ISGMR), can be used as experimental information to determine the incompressibility of nuclear matter K_∞ . The incompressibility of finite nucleus K_A is related with the breathing mode energy E_b as [1,2]

$$K_A = \frac{m \langle r^2 \rangle E_b^2}{\hbar^2}, \quad (2)$$

where $\langle r^2 \rangle$ is the mean square radius. By analogy of the semi-empirical mass formula, one can make an expansion of K_A with proton number Z , neutron number N and nucleon number A as

$$K_A(A, Z) = K_v + K_s A^{-1/3} + K_{vs} I^2 + K_c Z^2 A^{-4/3} + \dots, \quad (3)$$

where I is the asymmetry parameter defined by $I = (N - Z)/A$ and K_v , K_s , K_{vs} , and K_c , are the coefficients of volume, surface, volume symmetry, and Coulomb terms, respectively. The coefficients of several terms in Eq. (3) have been determined so as to reproduce empirical K_A values measured in many nuclei [1,2]. Other terms like curvature and deformation terms have also been included in the analysis [3]. Then, the coefficient of volume term K_v has been identified as the incompressibility of nuclear matter K_∞ in the limit of $A \rightarrow \infty$. Experimental data of ISGMR led the value of incompressibility of nuclear matter to $K_\infty \approx (210 \pm 30)$ MeV in the early 1980s [1,2,4,5]. However the value $K_\infty \approx (300 \pm 25)$ MeV was claimed by new experiments using isotopic chains of Sn and Sm nuclei [6]. A serious problem in the calculation of the value of K_∞ is that the coefficients of several terms used in Eq. (3) are not completely independent and cannot be determined uniquely from the experimental data. It was shown in Refs. [3,7] that the statistical error bar of the coefficients found in comparison with experimental data were so large as to make the result meaningless. It was also pointed out that there is a correlation between K_v and the third derivative of EOS of the nuclear matter at the saturation point [7]. This correlation suggests that there is an ambiguity to identify the volume term K_v in Eq. (3) with the nuclear matter incompressibility K_∞ , even in the limit of $A \rightarrow \infty$. Thus it might be concluded that reliable incompressibility of nuclear matter cannot be determined from the expansion formula (3) with the systematic data of ISGMR.

Recently, microscopic random phase approximation (RPA) calculations were performed by using both nonrelativistic Skyrme forces [8] and relativistic nonlinear σ model [9] in order to study the relation between the incompressibility and the excitation energy of ISGMR, in heavy nuclei like ^{90}Zr and ^{208}Pb . However, the two models give still controversial results for the incompressibility; the Skyrme RPA results agree well with the experimental data of ISGMR in

^{208}Pb with the interaction which has the incompressibility $K_\infty \approx 220$ MeV, while the results of relativistic RPA prefer a higher value for $K_\infty \approx (270-300)$ MeV.

It was pointed out that the saturation density of nuclear matter is very sensitive to the value of K_∞ and the model [10]. In this paper, we study the relation between incompressibility K_∞ of nuclear matter and properties of the nuclear density, especially the central density and the surface diffuseness. In Sec. II, the incompressibility and the saturation density of symmetric and asymmetric nuclear matter are discussed based on the relativistic mean field theory and the Skyrme Hartree-Fock model. In Sec. III, we show the correlation between the incompressibility and the surface diffuseness analytically by adding the derivative terms to the nuclear matter Hamiltonian density. Section IV is devoted to study the relation among the incompressibility of nuclear matter, the surface diffuseness and the central density of the

density distributions with the relativistic and the Skyrme self-consistent calculations. A summary is given in Sec. V.

II. SYMMETRIC AND ASYMMETRIC NUCLEAR MATTER AND NUCLEAR INCOMPRESSIBILITY

The incompressibility K_∞ of nuclear matter is defined by Eq. (1) as the second derivative of energy density with respect to the density at the saturation point. The content of the energy density \mathcal{H} depends on the theoretical model. In this paper, we adopt two models. One is the nonrelativistic Skyrme Hartree-Fock model and the other is the relativistic mean field theory.

At first, we show the formulation of the Skyrme Hartree-Fock model [11,12]. The Skyrme force V_{Sky} is an effective zero-range force with density and momentum dependent terms, which simulates the G matrix for nuclear Hartree-Fock calculations:

$$V_{\text{Sky}}(\vec{r}_1, \vec{r}_2) = t_0(1+x_0P_\sigma)\delta(\vec{r}_1-\vec{r}_2) + \frac{1}{2}t_1(1+x_1P_\sigma)\{\vec{k}'^2\delta(\vec{r}_1-\vec{r}_2) + \delta(\vec{r}_1-\vec{r}_2)\vec{k}^2\} + t_2(1+x_2P_\sigma)\vec{k}' \cdot \delta(\vec{r}_1-\vec{r}_2)\vec{k} + \frac{1}{6}t_3(1+x_3P_\sigma)\rho^\alpha(\vec{r})\delta(\vec{r}_1-\vec{r}_2) + iW(\vec{\sigma}_1+\vec{\sigma}_2) \cdot \vec{k}' \times \delta(\vec{r}_1-\vec{r}_2)\vec{k} \quad (4)$$

where $\vec{k} = (\vec{\nabla}_1 - \vec{\nabla}_2)/(2i)$ acting on the right and $\vec{k}' = -(\vec{\nabla}_1 - \vec{\nabla}_2)/(2i)$ acting on the left are the relative momentum, P_σ is the space exchange operator, $\vec{\sigma}$ is the Pauli spin matrix and ρ is the density at $\vec{r} = \frac{1}{2}(\vec{r}_1 + \vec{r}_2)$. The interaction parameters $t_0, x_0, t_1, x_1, t_2, x_2, t_3, x_3, \alpha$ are determined so as to reproduce nuclear matter saturation properties, while W gives the spin-orbit splitting.

The energy density for the Skyrme Hartree-Fock calculation is given by

$$\begin{aligned} \mathcal{H}(\rho_n, \rho_p) = & \frac{\hbar^2}{2m}(\tau_n + \tau_p) + \frac{1}{4}t_0(1-x_0)(\rho_n^2 + \rho_p^2) + t_0\left(1 + \frac{1}{2}x_0\right)\rho_n\rho_p + \frac{1}{12}t_3\left(1 + \frac{1}{2}x_3\right)\rho^{\alpha+2} - \frac{1}{12}t_3\left(\frac{1}{2} + x_3\right)\rho^\alpha(\rho_n^2 + \rho_p^2) \\ & + \frac{1}{8}[t_1(1-x_1) + 3t_2(1+x_2)](\rho_n\tau_n + \rho_p\tau_p) + \frac{1}{4}\left[t_1\left(1 + \frac{1}{2}x_1\right) + t_2\left(1 + \frac{1}{2}x_2\right)\right](\rho_n\tau_p + \rho_p\tau_n) \\ & - \frac{3}{32}[t_1(1-x_1) - t_2(1+x_2)](\rho_n\nabla^2\rho_n + \rho_p\nabla^2\rho_p) - \frac{1}{16}\left[3t_1\left(1 + \frac{1}{2}x_1\right) - t_2\left(1 + \frac{1}{2}x_2\right)\right](\rho_n\nabla^2\rho_p + \rho_p\nabla^2\rho_n) \\ & - \frac{1}{2}W(\rho\vec{\nabla}\vec{J} + \rho_n\vec{\nabla}\vec{J}_n + \rho_p\vec{\nabla}\vec{J}_p) + \mathcal{H}_{\text{Coul}}, \end{aligned} \quad (5)$$

where m is the nucleon mass, ρ_n (ρ_p) is the density of neutrons (protons) and $\rho = \rho_n + \rho_p$, while τ_n (τ_p) and \vec{J}_n (\vec{J}_p) are the kinetic energy and the spin densities of neutrons (protons), respectively.

In the following, we neglect the spin-orbit term W and the Coulomb term $\mathcal{H}_{\text{Coul}}$ for nuclear matter since they do not play important roles in the following discussion of this section. We use the extended Thomas Fermi approximation [13] for the kinetic energy density τ ,

$$\tau_{n(p)} = \frac{3}{5}(3\pi^2)^{2/3}\rho_{n(p)}^{5/3} + \frac{\eta}{36}\frac{(\nabla\rho_{n(p)})^2}{\rho_{n(p)}} + \frac{1}{3}\nabla^2\rho_{n(p)} \quad (6)$$

where the second and the third terms on the right-hand-side (RHS) are called Weizsäcker terms. Only nonderivative terms in Eqs. (5) and (6) are kept for calculations of the incompressibility of nuclear matter. The value of η is taken commonly to be $\eta = 1 \sim 2$ to obtain realistic surface energy coefficient for semi-infinite matter.

Next we discuss the formulation of the relativistic mean field theory. The following relativistic Lagrangian density \mathcal{L} is adopted for the interacting many-body system consisting of nucleons, scalar σ -, and vector ω -, and $\vec{\rho}$ - mesons, and photons [14-19],

$$\begin{aligned} \mathcal{L} = & \bar{\psi} \left(i \gamma^\mu \partial_\mu - M - g_\sigma \sigma - g_\omega \gamma^\mu \omega_\mu - g_\rho \gamma^\mu \vec{\tau} \vec{b}_\mu - e \gamma^\mu \frac{1 - \tau_3}{2} A_\mu \right) \psi \\ & + \frac{1}{2} (\partial_\mu \partial^\mu \sigma - m_\sigma^2 \sigma^2) - U(\sigma) + \frac{1}{2} m_\omega^2 \omega_\mu \omega^\mu - \frac{1}{4} F_{\mu\nu} F^{\mu\nu} + \frac{1}{2} m_\rho^2 \vec{b}_\mu \vec{b}^\mu - \frac{1}{4} \vec{G}_{\mu\nu} \vec{G}^{\mu\nu} - \frac{1}{4} H_{\mu\nu} H^{\mu\nu}, \end{aligned} \quad (7)$$

where ψ , σ , ω_μ , \vec{b}_μ , and A_μ are the nucleon, σ , ω , ρ meson fields and the electromagnetic field, respectively. The γ^μ is the Dirac matrix, $\vec{\tau}$ is the isospin matrix, $F_{\mu\nu} \equiv \partial_\mu \omega_\nu - \partial_\nu \omega_\mu$, $\vec{G}_{\mu\nu} \equiv \partial_\mu \vec{b}_\nu - \partial_\nu \vec{b}_\mu$, $H_{\mu\nu} \equiv \partial_\mu A_\nu - \partial_\nu A_\mu$. The g_σ , g_ω , and g_ρ are the coupling constants between nucleons and σ , ω , and ρ mesons, respectively, while $e^2/4\pi = 1/137$ is the finestructure constant. The m_σ , m_ω , m_ρ , and M are the masses of σ -, ω -, ρ - mesons and nucleons, respectively. The $U(\sigma)$ is a nonlinear potential of σ mesons [20]:

$$U(\sigma) = \frac{1}{3} g_1 \sigma^3 + \frac{1}{4} g_2 \sigma^4, \quad (8)$$

where the g_1 and g_2 are parameters of the potential. The Dirac equation for nucleons and the Klein-Gordon equations for mesons are derived by the classical variational principle with the time reversal symmetry and the charge conservation:

$$\begin{aligned} & \left[-i \vec{\alpha} \vec{\nabla} + \beta M^* + g_\omega \omega(\vec{r}) + g_\rho \tau_3 b(\vec{r}) + e \frac{1 - \tau_3}{2} A(\vec{r}) \right] \psi_i(\vec{r}) \\ & = \varepsilon_i \psi_i(\vec{r}) \end{aligned} \quad (9)$$

$$\begin{aligned} (-\nabla^2 + m_\sigma^2) \sigma(\vec{r}) &= -g_\sigma \rho_s(\vec{r}) - g_1 \sigma^2(\vec{r}) - g_2 \sigma^3(\vec{r}) \\ &\times (-\nabla^2 + m_\omega^2) \omega(\vec{r}) = g_\omega \rho_B(\vec{r}) \\ &\times (-\nabla^2 + m_\rho^2) b(\vec{r}) = g_\rho \rho_3(\vec{r}) \\ -\nabla^2 A(\vec{r}) &= e \rho_p(\vec{r}), \end{aligned} \quad (10)$$

where $\vec{\alpha}$ and β are defined by $\vec{\alpha} = \begin{pmatrix} 0 & \vec{\sigma} \\ \vec{\sigma} & 0 \end{pmatrix}$ and $\beta = \begin{pmatrix} I & 0 \\ 0 & -I \end{pmatrix}$ with the Pauli matrices $\vec{\sigma}$ and the 2×2 unit matrix I , respectively. ρ_B and ρ_s are the baryon and the scalar densities, respectively, while $\rho_3 = \rho_n - \rho_p$. The effective mass M^* is defined by $M^* = M + g_\sigma \sigma$. By using Eqs. (9) and (10), the static Hamiltonian density in the nuclear matter can be obtained as

$$\begin{aligned} \mathcal{H} = & \frac{2}{(2\pi)^3} \left[\int_0^{k_{F_p}} + \int_0^{k_{F_n}} \right] (k^2 + M^{*2})^{1/2} d^3k + g_\omega \omega \rho_B \\ & - \frac{1}{2} m_\omega^2 \omega^2 + U(\sigma) + \frac{1}{2} m_\sigma^2 \sigma^2 + g_\rho b \rho_3 - \frac{1}{2} m_\rho^2 b^2, \end{aligned} \quad (11)$$

where k_{F_n} and k_{F_p} are the Fermi momenta for neutrons and protons, respectively. Furthermore, the baryon density ρ_B is given by $\rho_B = 2k_F^3/(3\pi^2)$ using the Thomas Fermi approximation. The static Klein-Gordon equations in the nuclear matter become

$$\begin{aligned} m_\sigma^2 \sigma &= -g_\sigma \rho_s - g_1 \sigma^2 - g_2 \sigma^3 \\ m_\omega^2 \omega &= g_\omega \rho_B \\ m_\rho^2 b &= g_\rho \rho_3, \end{aligned} \quad (12)$$

where the scalar density ρ_s in the nuclear matter is given by

$$\rho_s = \frac{2}{(2\pi)^3} \left[\int_0^{k_{F_n}} + \int_0^{k_{F_p}} \right] \frac{M^*}{(k^2 + M^{*2})^{1/2}} d^3k. \quad (13)$$

We neglected the Coulomb term similarly to the case of Skyrme Hartree-Fock calculations.

For the symmetric nuclear matter $N=Z$, the neutron density ρ_n and the proton density ρ_p are taken as a half of the total density ρ . In the case of the asymmetric nuclear matter, the ratio between the neutron density and the proton density is determined to be the same as that of the neutron and proton numbers. Figures 1(a) and 1(b) show the change of the incompressibility K_∞ and the saturation density ρ_0 of nuclear matter as a function of asymmetry parameter I , respectively. The parameter sets used are NL1 [17] and NLSH [21] in the relativistic mean field calculations, and SGII [22] and SIII [23] in the Skyrme Hartree-Fock calculations. The incompressibilities of the NL1 and NLSH are $K_\infty = 211$ and $K_\infty = 355$ MeV, respectively, while the SGII and SIII have $K_\infty = 217$ and $K_\infty = 356$ MeV, respectively. The results for the NL1, NLSH, SGII, and SIII parameters are shown by the solid, dashed, dotted, and dot-dashed lines, respectively. It is interesting to notice in Fig. 1(a) that the I dependence of the incompressibility for SGII and NL1, which have almost the same small K_∞ values at $I=0.0$, is rather weak, while the other two interactions SIII and NLSH have stronger I dependence. A similar I dependence to those of SGII and NL1 is found in the asymmetric nuclear matter calculations with relativistic nucleon-nucleon interactions [24].

The I dependence of the central density shown in Fig. 1(b) is somewhat different from that of K_∞ in Fig. 1(a). The saturation densities ρ_0 of NL1, NLSH, and SGII forces decrease rather rapidly as the asymmetry parameter I increases, but that of SIII stays almost constant.

Figures 2(a) and 2(b) show the correlation between the incompressibility K_∞ and the saturation density ρ_0 for 16 different interactions in the cases of $I=0.0$ and $I=0.6$. The results for the Skyrme Hartree-Fock model and relativistic mean field theory are shown by filled circles and open circles, respectively.

At $I=0.0$, there is a tendency that the parameter set with larger incompressibility gives smaller saturation density. The interactions Skb and SkM* shown in the brackets in Fig. 2(a) have the same results with those for the Ska and SkM, respectively. At $I=0.6$, the correlation between the incom-

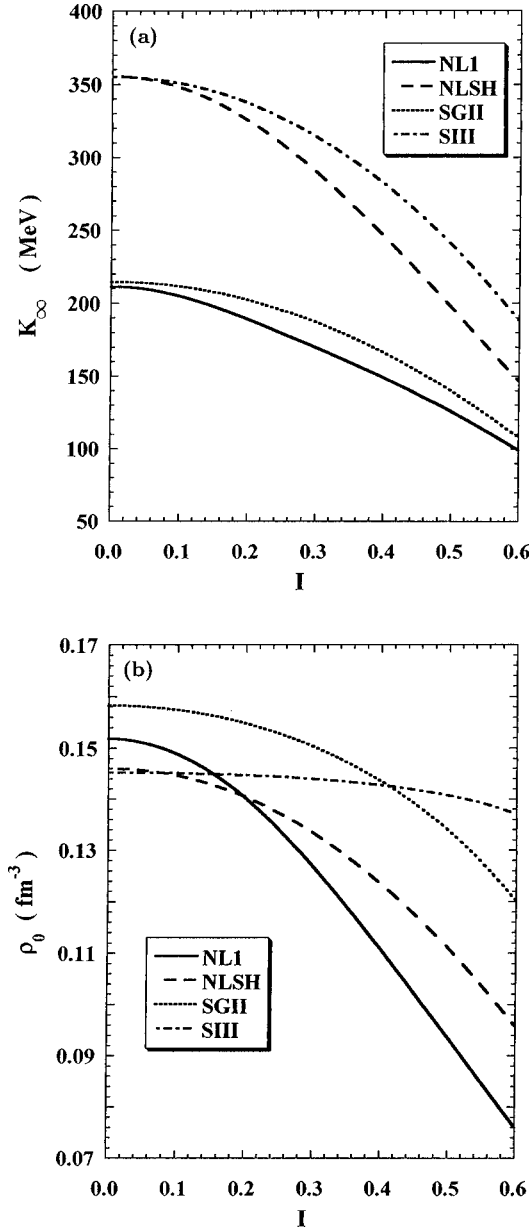


FIG. 1. (a) Asymmetry parameter $I=(N-Z)/A$ dependence of the incompressibility K_∞ . (b) I dependence of the saturation density ρ_0 of asymmetric nuclear matter. The solid and dashed lines are calculated by NL1 and NLSH interactions in the relativistic mean field theory, respectively, while the dotted and dot-dashed lines are obtained by SGII and SIII parameter sets of Skyrme forces, respectively.

pressibility and the central density is opposite; the parameter set with larger incompressibility gives larger saturation density. The correlation between the incompressibility K_∞ and the saturation density ρ_0 of nuclear matter is shown in Fig. 3 where the asymmetry parameter I is changed from 0.0 to 0.6. The change of K_∞ is largest for SIII as a function of I , while the saturation density changes only slightly [24]. The opposite extreme is the NL1 set, for which the saturation density drastically changes from $\rho_0=0.152$ to $\rho_0=0.076$ as I changes from 0.0 to 0.6, while the incompressibility K_∞ changes only moderately from 211 MeV to 99 MeV.

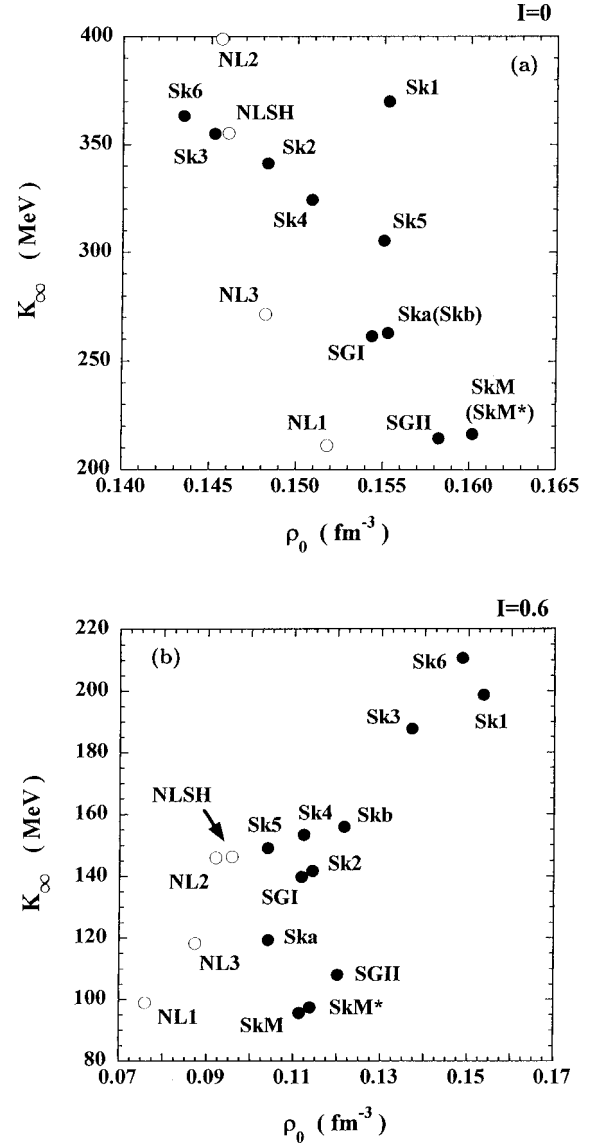


FIG. 2. Correlation between the incompressibility K_∞ and the saturation density ρ_0 : (a) is the case of $I=0.0$ and (b) is the case of $I=0.6$. Filled circles are the results with the parameter sets of Skyrme forces and the opened circles are those with the parameter sets of relativistic mean field theory.

III. INCOMPRESSIBILITY IN SEMI-INFINITE MATTER

We now discuss the relation between the incompressibility K_∞ of nuclear matter and the surface diffuseness of the density distribution in semi-infinite nuclear matter. At first, we derive analytic formulas by using the Thomas Fermi approximation for the kinetic energy density. The Hamiltonian density of nuclear matter near the saturation density ρ_0 has been parametrized in Refs. [11,13] as

$$\mathcal{H}=E_1\rho\left(1-\frac{\rho}{\rho_0}\right)^2-E_0\rho, \quad (14)$$

where E_0 is the energy at the saturation density ρ_0 and E_1 is a coefficient proportional to the incompressibility. Namely, $E_1=K_\infty/18$ can be derived by the relation between the Hamiltonian density \mathcal{H} and the incompressibility K_∞ in Eq.

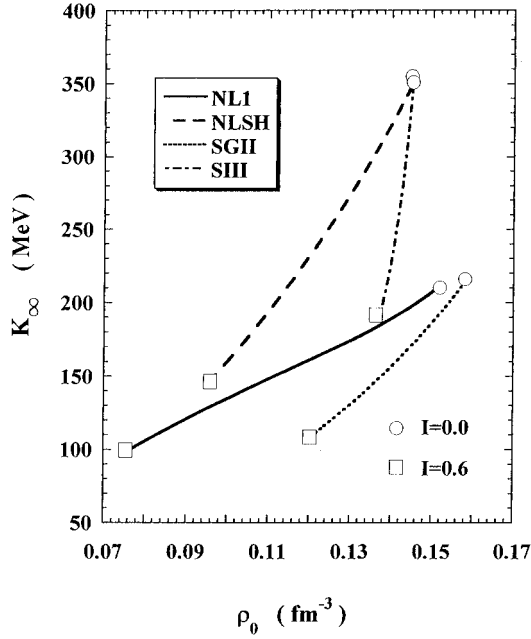


FIG. 3. Correlation between the incompressibility K_∞ and the saturation density ρ_0 . The solid, dashed, dotted, and dot-dashed lines are calculated by NL1, NLSH, SGII, and SIII interactions, respectively. The asymmetry parameter I is changed from $I=0.0$ to $I=0.6$, continuously.

(1). Using the extended Thomas Fermi approximation (6), the Hamiltonian density (5) is then given by

$$\mathcal{H} = \frac{K_\infty}{18} \rho_0 y (1-y)^2 - E_0 \rho_0 y + A \rho_0 \frac{(\nabla y)^2}{y} + B \rho_0^2 (\nabla y)^2, \quad (15)$$

where $y \equiv \rho/\rho_0$. The constant A is determined by the coefficients of Weizsäcker terms of Eq. (6), while constant B is given by the Skyrme force parameters:

$$A = \frac{\hbar^2 \eta}{72m} \quad (16)$$

$$B = \frac{1}{576} [\{3(\eta+15)t_1 + (\eta-21)t_2(5+4x_2)\} + \{-(\eta+15)t_1(1+2x_1) + (\eta-21)t_2(1+2x_2)\}I^2].$$

Notice that the coefficient B contains the asymmetry parameter I . The Hartree-Fock condition for the saturation density is given by the Euler-Lagrange equation,

$$\frac{K_\infty}{18} \rho_0 (3y^2 - 4y + 1) - E_0 \rho_0 + A \rho_0 \frac{(\nabla y)^2}{y^2} - 2\rho_0 \left(B \rho_0 + \frac{A}{y} \right) \nabla^2 y = \lambda. \quad (17)$$

The Lagrange multiplier λ becomes $-E_0 \rho_0$ in the limit of nuclear matter, i.e., $y \rightarrow 1$ and $\nabla y = \nabla^2 y = 0$. In the model of semi-infinite system, the derivatives in Eq. (17) are reduced

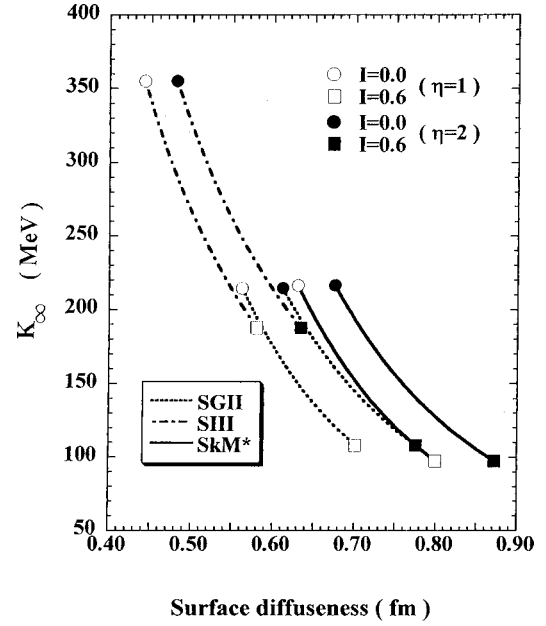


FIG. 4. Correlation between the incompressibility K_∞ and the surface diffuseness a with SGII (the dotted line), SIII (the dot-dashed line), and SkM* (the solid line) forces. The asymmetry parameter I is changed from $I=0.0$ to $I=0.6$, continuously. The results for two different values of the multiplication factor to the Weizsäcker term, $\eta=1$ and 2 , are shown with the open and the closed symbols, respectively.

to one dimensional differentiations; $\nabla y \rightarrow dy/dx$ and $\nabla^2 y \rightarrow d^2 y/dx^2$. Equation (17) can then be rewritten as

$$\frac{dy}{dx} = - \sqrt{\frac{K_\infty}{18(B\rho_0 y + A)}} y(1-y). \quad (18)$$

In order to relate the incompressibility K_∞ and the surface diffuseness, we assume a Fermi-type function $y = (1 + e^{(x-R)/a})^{-1}$ for the density distribution. In order to determine the surface diffuseness, Eq. (18) is integrated over x from $-\infty$ to $+\infty$ and, correspondingly, y from 1 to 0 . Using the integration formulas,

$$\int_{-\infty}^{\infty} dx y(1-y) = a \quad (19)$$

and

$$\int_0^1 dy \sqrt{y + \alpha} = \frac{2}{3} [(1 + \alpha)^{3/2} - \alpha^{3/2}] \quad (20)$$

we obtain

$$a = \frac{2}{\rho_0} \sqrt{\frac{2B}{K_\infty}} \left[\left(\rho_0 + \frac{A}{B} \right)^{3/2} - \left(\frac{A}{B} \right)^{3/2} \right]. \quad (21)$$

Equation (21) shows that the surface diffuseness a is inversely proportional to the square root of the incompressibility K_∞ .

Figure 4 shows the correlation between the incompressibility K_∞ and the surface diffuseness a for the SGII (the dotted line), SIII (the dot-dashed line) and SkM* [25] (the

TABLE I. Root mean square radii of Sn isotopes calculated by using the relativistic mean field theory with two parameter sets, NL1 [17] and NLSH [21]. r_n , r_c , and r_m are the root mean square neutron, charge, and matter radii, respectively, while $r_n - r_p$ is the difference between the neutron and proton radii. Experimental data are taken from Ref. [29]. All values are given in units of fm.

Nuclei	NL1					NLSH				
	r_n	r_c	(Expt.)	$r_n - r_p$	r_m	r_n	r_c	(Expt.)	$r_n - r_p$	r_m
¹⁰⁰ Sn	4.311	4.455		-0.072	4.347	4.314	4.460		-0.074	4.351
¹⁰⁴ Sn	4.455	4.504		0.023	4.444	4.433	4.500		0.004	4.431
¹⁰⁸ Sn	4.581	4.545		0.107	4.531	4.529	4.537		0.063	4.500
¹¹² Sn	4.682	4.581	4.586	0.171	4.606	4.627	4.569	4.586	0.129	4.570
¹¹⁶ Sn	4.778	4.614	4.619	0.234	4.679	4.716	4.598	4.619	0.188	4.636
¹²⁰ Sn	4.860	4.643	4.646	0.287	4.743	4.791	4.626	4.646	0.235	4.695
¹²⁴ Sn	4.934	4.669	4.670	0.334	4.802	4.858	4.652	4.670	0.275	4.749
¹²⁸ Sn	5.007	4.695		0.380	4.862	4.917	4.678		0.308	4.799
¹³² Sn	5.094	4.722		0.440	4.932	4.964	4.703		0.330	4.842
¹³⁶ Sn	5.227	4.759		0.536	5.036	5.121	4.737		0.452	4.959
¹⁴⁰ Sn	5.340	4.793		0.614	5.129	5.221	4.769		0.520	5.042
¹⁵⁰ Sn	5.563	4.881		0.748	5.326	5.426	4.851		0.642	5.221
¹⁶⁰ Sn	5.788	4.967		0.886	5.527	5.592	4.928		0.729	5.375

solid line) forces, respectively, in which the asymmetry parameter I is changed from 0.0 to 0.6. The η in Eq. (16) is taken to be $\eta=1$ and $\eta=2$. The results with $\eta=1$ and $\eta=2$ in Fig. 4 show qualitatively the same K_∞ dependence, but qualitatively the surface diffuseness with $\eta=2$ is about 10% larger than that for $\eta=1$ for all interactions. There is a clear difference in the surface diffuseness a given by the SGII and SGIII forces reflecting the incompressibility dependence of a in Eq. (21). It is also interesting to notice that the SkM* force gives a larger surface diffuseness than the SGII force despite the fact that they have almost the same K_∞ value. Experimental data of electron scattering and the x-ray measurements of μ -onic atoms are consistent with the surface diffuseness $a=0.54$ fm for all stable nuclei $A > 16$ [26]. The calculated value of SGII with $\eta=1$ at $I=0$ is close to the empirical value, but somewhat larger at $I > 0$.

IV. INCOMPRESSIBILITY OF Sn ISOTOPES IN THE RELATIVISTIC AND NONRELATIVISTIC MEAN FIELD PLUS BCS CALCULATIONS

In this section, we present the results of relativistic and nonrelativistic mean field calculations supplemented by the BCS theory for the pairing correlation for Sn isotopes. We use the original Hamiltonian density (5) for the nonrelativistic Skyrme Hartree Fock calculations without introducing the extended Thomas Fermi approximation, while Eqs. (9) and (10) are adopted for the relativistic mean field calculations. In both calculations, the pairing correlation is then taken into account in the BCS theory by solving the gap equations for the neutrons and protons taking the strengths of the pairing interactions G_p and G_n from [27,28]. See Ref. [28] for details of the numerical calculations concerning the BCS approximation.

In subsection A, we discuss the isotope dependence of the radii of the neutron and the proton distributions, and of the density profile for various parameter sets in the relativistic and nonrelativistic calculations. In subsection B, we use

these results to discuss the relation among the incompressibility of nuclear matter, the surface diffuseness, and the central density of finite nuclei. To this end, we fit the calculated density distribution by the Fermi-type density function.

A. Radii and density profile

Tables I and II show the results of relativistic and nonrelativistic calculations of the radii for various Sn isotopes ranging from neutron deficient to neutron rich regions. The NL1 and NLSH, and the SGII and SGIII parameter sets have been used for the relativistic and nonrelativistic calculations, respectively. The r_n and r_p are the root mean square radii of neutrons and protons, respectively, while the r_m is the root mean matter radius. The charge radii r_c has been obtained by convoluting the Gaussian proton charge distribution with the root mean square radius 0.8 fm to the proton density. Figure 5 shows the root mean square charge radius r_c as a function of the asymmetry parameter I for the NL1 (the open circles), NLSH (the open squares), SGII (the filled circles), and SGIII (the filled squares) parameter sets. Qualitatively, the increase of the empirical radius r_c with I [29] is well reproduced by all four interactions. Among them, NL1, NLSH, and SGII give satisfactory results quantitatively as well, while the SGIII parameter set gives systematically larger charge radius by 0.07 fm on average than the experimental value. All the four calculations predict a kink in the change of the charge radius with I at the doubly closed nucleus ¹³²Sn. This is similar to that observed in the isotope shift of Pb nuclei [28]. It will be interesting to experimentally confirm this kink at ¹³²Sn.

Figures 6(a) and 6(b) show the charge density distributions of ^{112,116,120,124}Sn calculated with the NL1 and NLSH, and SGII and SGIII interactions, respectively. The dotted and dashed lines are the calculated results, while the solid line is the experimental data. The central density distribution is smooth in experimental data for all isotopes, while the cal-

TABLE II. Root mean square radii of Sn isotopes calculated by using Skyrme Hartree-Fock model with two parameter sets, SGII [22] and SIII [23]. r_n , r_c , and r_m are the root mean square neutron, charge, and matter radii, respectively, while $r_n - r_p$ is the difference between the neutron and proton radii. Experimental data are taken from Ref. [29]. All values are given in units of fm.

Nuclei	SGII					SIII				
	r_n	r_c	(Expt.)	$r_n - r_p$	r_m	r_n	r_c	(Expt.)	$r_n - r_p$	r_m
^{100}Sn	4.330	4.496		-0.086	4.374	4.388	4.544		-0.076	4.426
^{104}Sn	4.421	4.533		-0.033	4.437	4.476	4.583		-0.028	4.490
^{108}Sn	4.499	4.567		0.010	4.495	4.554	4.620		0.012	4.548
^{112}Sn	4.571	4.600	4.586	0.048	4.550	4.625	4.654	4.586	0.047	4.604
^{116}Sn	4.639	4.632	4.619	0.083	4.603	4.691	4.685	4.619	0.080	4.657
^{120}Sn	4.704	4.660	4.646	0.118	4.656	4.753	4.713	4.646	0.110	4.707
^{124}Sn	4.764	4.685	4.670	0.149	4.704	4.810	4.739	4.670	0.137	4.755
^{128}Sn	4.819	4.708		0.176	4.751	4.863	4.764		0.161	4.801
^{132}Sn	4.870	4.730		0.200	4.795	4.913	4.788		0.184	4.844
^{136}Sn	4.956	4.765		0.249	4.866	4.992	4.819		0.228	4.910
^{140}Sn	5.032	4.799		0.289	4.930	5.063	4.851		0.265	4.970
^{150}Sn	5.198	4.884		0.367	5.079	5.214	4.929		0.334	5.105
^{160}Sn	5.347	4.959		0.436	5.214	5.345	4.997		0.392	5.226

culated one shows fluctuations. The surface part of the experimental density is well reproduced by the NL1 and SGII interactions, while the other two interactions show some discrepancies.

Figures 7(a) and 7(b) show the neutron and proton density distributions of $^{100,120,140,160}\text{Sn}$ calculated with the NL1, NLSH, SGII, and SIII forces, respectively. In each figure, we compare the results of relativistic and nonrelativistic calculations using forces with a similar incompressibility, i.e., in

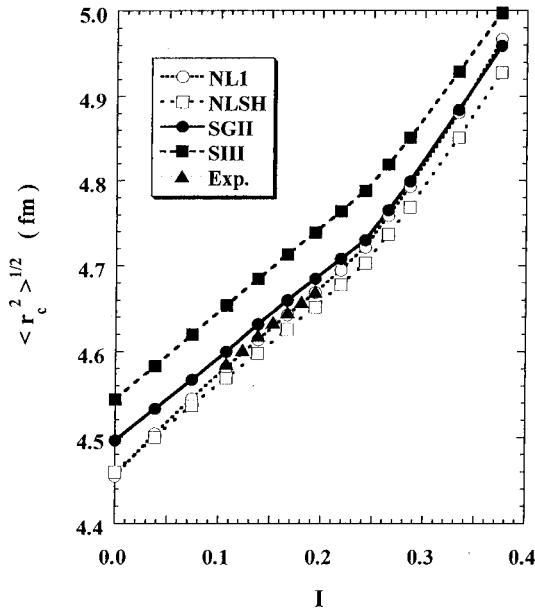


FIG. 5. Asymmetry parameter I dependence of the charge radii of Sn isotopes. The open circles and squares are calculated by the relativistic mean field theory with NL1 and NLSH interactions, respectively, while the filled circles and squares are calculated by the Skyrme Hartree-Fock model with SGII and SIII interactions, respectively. Experimental data (filled triangles) are taken from Ref. [29].

Fig. 7(a), we compare the results obtained by the NL1 and SGII interactions which have relatively small incompressibilities, while the results of the NLSH and SIII, which have larger incompressibilities, are compared in Fig. 7(b).

As seen in Tables I and II, both the neutron and proton radii increase with the neutron number. The central density of neutrons increases from $A=100$ to $A=120$, and stays almost constant for heavier isotopes, while the neutron skin grows from $A=120$ to $A=160$. The central proton density decreases with the neutron number, because the strong neutron-proton interaction extends the proton distribution outward. If one compares Figs. 7(a) and 7(b), one notices that the interactions with the smaller incompressibilities, i.e., those shown in Fig. 7(a), lead to a larger surface diffuseness. This is consistent with what we discussed in the previous section using Eq. (21). However, if one sees more closely, there are noticeable differences between the relativistic and nonrelativistic calculations in each figure, especially for the ^{140}Sn and ^{160}Sn isotopes. For example, the neutron surface thickness given by the SGII force is smaller than that given by the NL1 set and this difference becomes larger for heavier isotopes. A similar trend can be seen in Fig. 7(b), where one sees that the neutron surface thickness given by the nonrelativistic calculations using the SIII force is systematically smaller than that given by the relativistic calculations using the NLSH set.

B. Correlations among the incompressibility, central density, and surface diffuseness

We now discuss the correlations among the incompressibility, the surface diffuseness and the central density of finite nuclei. To this end, we fit the calculated density distribution $\rho(r) = \rho_n(r) + \rho_p(r)$ for each isotope with the Fermi-type function $\rho(r) = \rho_0 / (1 + e^{(r-R)/a})$. We use the equation $A = (4\pi/3) \rho_0 R^3 \{1 + \pi^2 (a/R)^2\}$ to guarantee the mass number A conservation and consider r^2 times the density instead

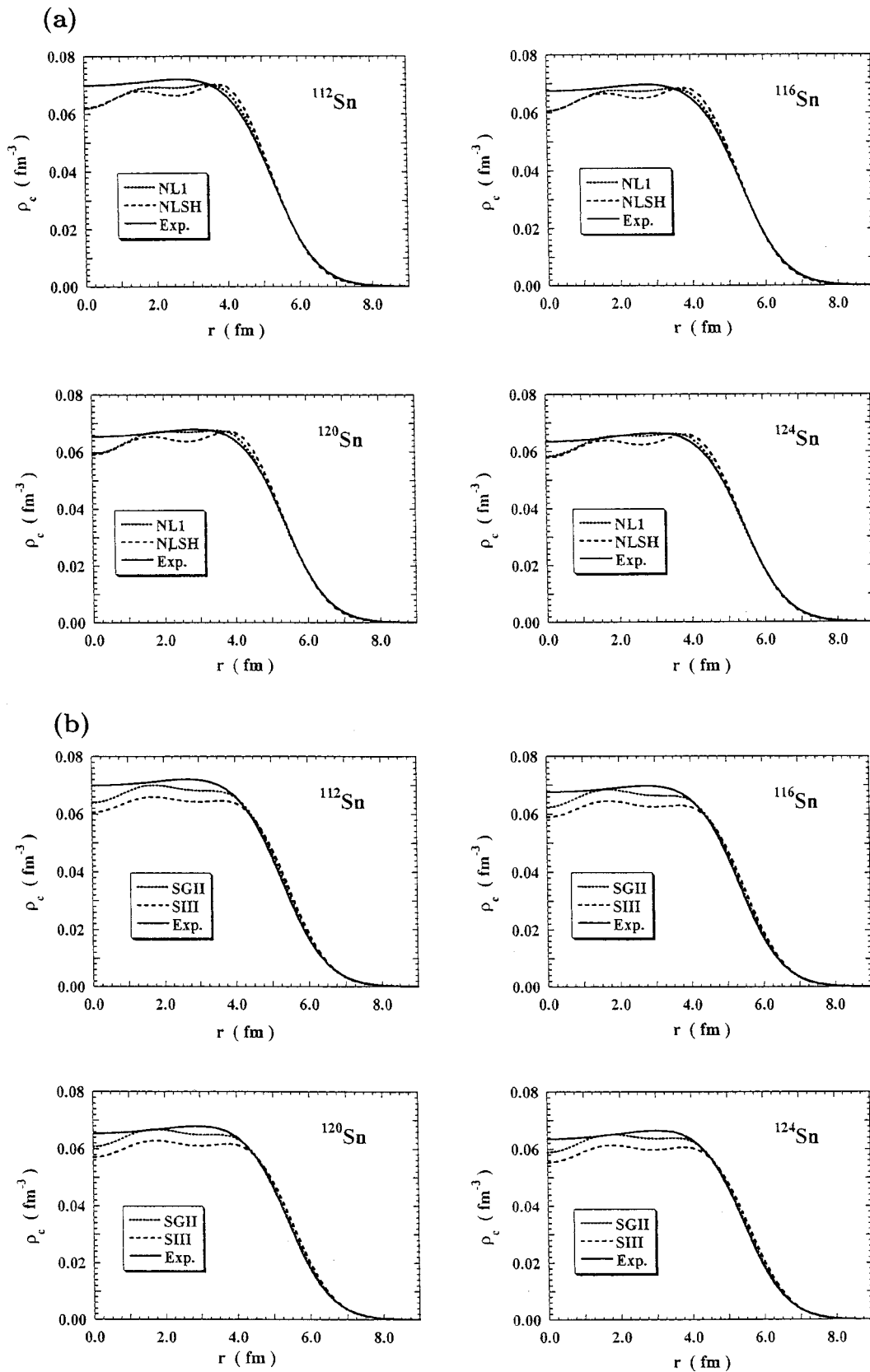


FIG. 6. Charge density distributions of $^{112,116,120,124}\text{Sn}$; (a) with NL1 and NLSH, and (b) with SGII and SIII interactions. The dotted, dashed, and solid lines show calculated results and experimental data, respectively. Experimental data are taken from Ref. [29].

of the density itself in order to extract the surface diffuseness without being suffered from the fluctuations in the theoretical density distribution near $r=0$.

Figures 8(a) and 8(b) show the correlation between the obtained central density and the incompressibility K_∞ and that between the surface diffuseness and the incompressibil-

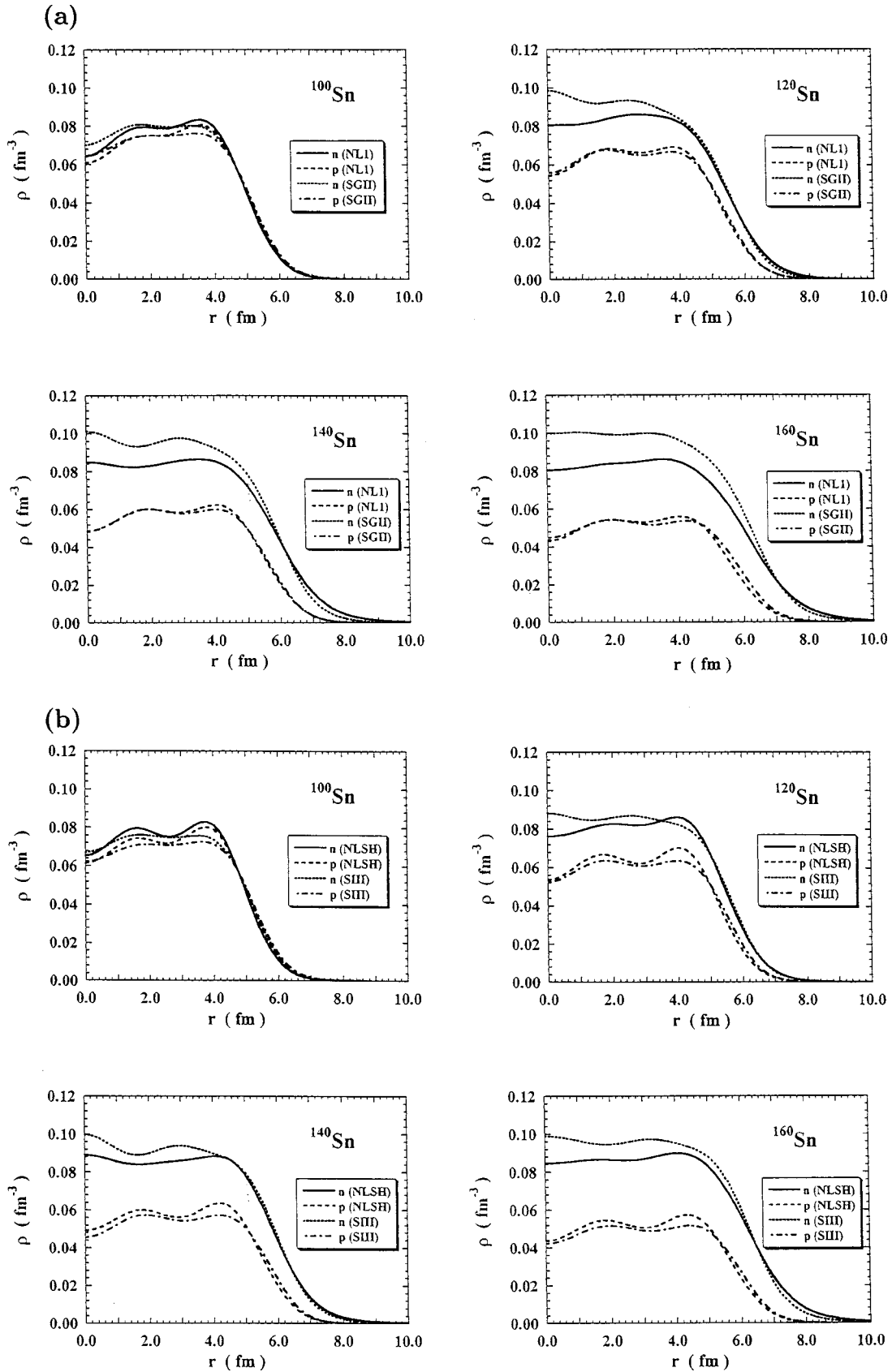


FIG. 7. Neutron and proton density distributions of $^{100,120,140,160}\text{Sn}$; (a) with NL1 and SGII, and (b) with NLSH and SIII, respectively. The solid and dashed (dashed and dot-dashed) lines show densities of neutrons (protons), respectively.

ity K_∞ , respectively, where K_∞ has been determined for each isotope from Fig. 1(a) at the corresponding I value. The results are obtained by the relativistic calculations with the

NL1 (the open circles) and NLSH (the open squares) parameter sets, and by the nonrelativistic calculations with the SGII (the filled circles) and SIII (the filled squares) forces.

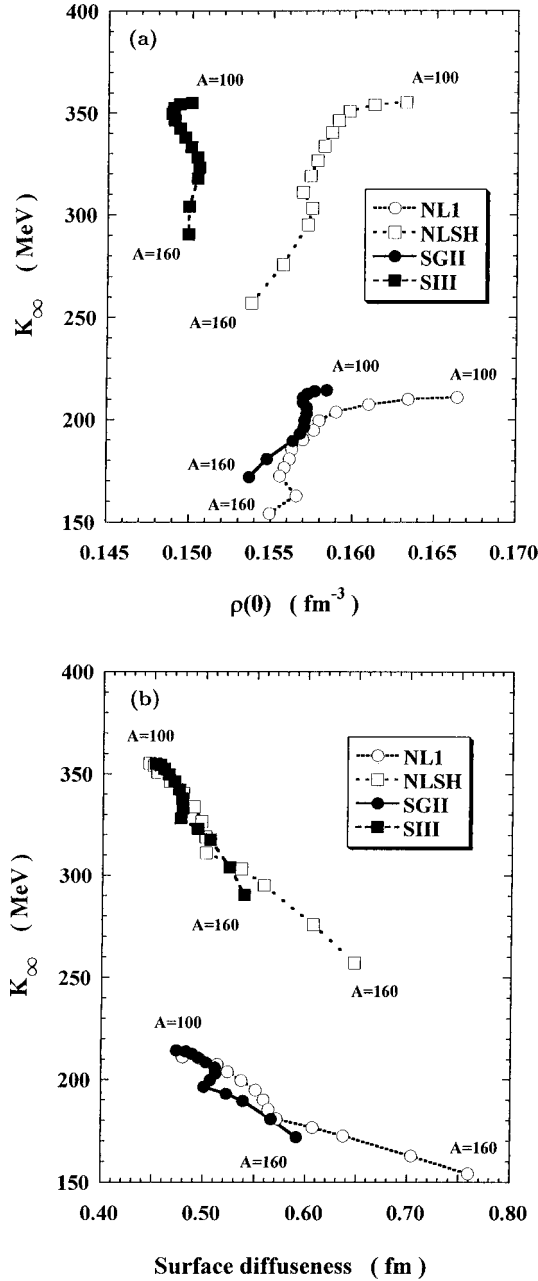


FIG. 8. (a) Correlation between the incompressibility K_∞ and the central density in Sn isotopes. (b) Correlation between the incompressibility K_∞ of asymmetric nuclear matter and the surface diffuseness in Sn isotopes. The open circles and squares are calculated by the relativistic mean field theory with NL1 and NLSH interactions, respectively, while the filled circles and squares are calculated by the Skyrme Hartree-Fock model with SGII and SIII interactions, respectively. The results of 13 Sn isotopes are shown by changing 4 neutrons in succession between $A = 100$ and $A = 140$ and 10 neutrons in succession between $A = 140$ and $A = 160$.

The 13 Sn isotopes are studied by changing 4 neutrons in succession between $A = 100$ and $A = 140$ and 10 neutrons in succession between $A = 140$ and $A = 160$. The incompressibility K_∞ is the largest for ^{100}Sn and the smallest for ^{160}Sn .

The correlation between the incompressibility K_∞ and the central density in Fig. 8(a) is found to be very analogous to that between K_∞ and the saturation density for nuclear matter

shown in Fig. 3. In general, a stronger isotope dependence of the central density $\rho(0)$ is predicted in relativistic calculations than that in nonrelativistic Skyrme Hartree-Fock calculations.

Figure 8(b) shows the correlation between the surface diffuseness a and K_∞ . The surface diffuseness monotonically increases with the neutron number except for the isotopes in the vicinity of the double magic nucleus ^{132}Sn , while the incompressibility K_∞ decreases. Therefore, there is a clear correlation between a and K_∞ irrespective of the relativistic or non-relativistic calculations, and of the details of the parameter sets within each approach.

Moreover, the figure shows that the NL1 set and the SGII force which have almost the same small K_∞ value have very similar correlation between K_∞ and a not only qualitatively, but also quantitatively for the isotopes between $A = 100$ and 132, though the relativistic calculations predict much larger surface diffuseness for heavier isotopes. A similar situation holds for the NLSH set and the SIII force which have almost the same large K_∞ value. The dependence of the central density and the surface diffuseness on the asymmetry parameter I shown in Figs. 8(a) and 8(b) will be useful to distinguish various theoretical models through a systematic experimental study of the density distributions of Sn-isotopes.

V. SUMMARY

We studied the incompressibility of asymmetric nuclear matter in relation to the saturation density and the surface diffuseness. First, the analytic expressions of the Hamiltonian density in the relativistic mean field theory and in the Skyrme Hartree-Fock theory have been used to discuss the asymmetry parameter I dependence of the saturation density and its connection with the incompressibility K_∞ . We found that the saturation density is smaller for the interaction with larger incompressibility in the case of $I = 0.0$. On the other hand, at $I = 0.6$, the correlation is opposite; the saturation density is larger for the interaction with larger incompressibility. These results for the saturation density hold irrespectively of the relativistic or nonrelativistic models. We studied also the relation between the incompressibility of asymmetric nuclear matter and the surface diffuseness of the density distribution by using the extended Thomas Fermi approximation. We obtained the analytic relation in which the surface diffuseness is inversely proportional to the root of the incompressibility K_∞ and also depends on the asymmetry parameter I . Next we showed the correlations between the incompressibility of asymmetric nuclear matter and the surface diffuseness, and between the incompressibility and the central density in the relativistic mean field calculations with NL1 and NLSH interactions and also in the Skyrme Hartree-Fock calculations with SGII and SIII interactions. We extracted the surface diffuseness and the central densities by fitting the calculated nuclear densities of 13 Sn isotopes with the Fermi-type function. In these analyses, we found that the correlation between the incompressibility of asymmetric nuclei and the central density of nuclei is similar to that between the incompressibility and the saturation density of asymmetric nuclear matter. It was also found that there is a clear model dependence of the correlation between the in-

compressibility of asymmetric nuclear matter and the central density, even for the interactions which have almost the same incompressibility. On the other hand, the two models give a very similar correlation between the incompressibility and the surface diffuseness for the isotopes $A = 100\text{--}160$, for the interactions with almost the same incompressibilities for symmetric nuclear matter. This correlation is very different for the interaction with different incompressibility in the same model. The above correlations could be useful to pin down the validity of the models and also the interactions in comparison with future experimental data of density distributions in nuclei near drip lines.

ACKNOWLEDGMENTS

We would like to thank M. Di Toro for stimulating discussions in the early stage of this work. One of the authors (S.Y.) would like to thank M. Tanifuji, Y. Koike, and S. Ishikawa for encouragement. This project was partially supported by Grant-in-Aid for Scientific Research on General Areas (No. 09640369) from the Ministry of Education, Science, Culture and Sports, and also by the Grant-in-Aid for General Scientific Research, Contract No. 08640380, Monbusho International Scientific Research Program: Joint Research, Contract No. 09044051, from the Japanese Ministry of Education, Science and Culture.

-
- [1] J.P. Blaizot, Phys. Rep. **64**, 171 (1980).
 [2] O. Bohigas, A.M. Lane, and J. Martorell, Phys. Rep. **51**, 267 (1979).
 [3] S. Shlomo and D.H. Youngblood, Phys. Rev. C **47**, 529 (1993).
 [4] H. Krivine, J. Treiner, and O. Bohigas, Nucl. Phys. **A336**, 155 (1980).
 [5] J. Treiner, H. Krivine, O. Bohigas, and J. Martorell, Nucl. Phys. **A371**, 253 (1981).
 [6] M.M. Sharma *et al.*, Phys. Rev. C **38**, 2562 (1988).
 [7] J.M. Pearson, Phys. Lett. B **271**, 12 (1991).
 [8] I. Hamamoto, H. Sagawa, and X.Z. Zhang, Phys. Rev. C **56**, 3121 (1997).
 [9] Z. Ma, H. Toki, Nguyen.Van. Giai, and M. L'Huillier, Phys. Rev. C **55**, 2385 (1997).
 [10] K. Oyamatsu *et al.*, Riken report, 1997.
 [11] T.H.R. Skyrme, Philos. Mag. **1**, 1043 (1956); Nucl. Phys. **9**, 615 (1959).
 [12] D. Vautherin and D.M. Brink, Phys. Rev. C **5**, 626 (1972).
 [13] M. Brack, C. Guet, and H.-B. Håkansson, Phys. Rep. **123**, 275 (1985).
 [14] J.D. Walecka, Ann. Phys. (N.Y.) **83**, 469 (1974).
 [15] C.J. Horowitz and B.D. Serot, Nucl. Phys. **A368**, 503 (1981).
 [16] B.D. Serot and J.D. Walecka, Adv. Nucl. Phys. **16**, 1 (1986).
 [17] P.G. Reinhard, M. Rufa, J. Maruhn, W. Greiner, and J. Friedrich, Z. Phys. A **323**, 13 (1986).
 [18] Y.K. Gambhir, P. Ring, and A. Thimet, Ann. Phys. (N.Y.) **198**, 132 (1990).
 [19] B.D. Serot, Rep. Prog. Phys. **55**, 1855 (1992); P.G. Reinhard, *ibid.* **52**, 439 (1992).
 [20] J. Boguta and A.R. Bodmer, Nucl. Phys. **A292**, 413 (1977).
 [21] M.M. Sharma, M.A. Nagarajan, and P. Ring, Phys. Lett. B **312**, 377 (1993).
 [22] Nguyen van Giai and H. Sagawa, Phys. Lett. **106B**, 379 (1981).
 [23] M. Beiner, M. Flocard, N. van Giai, and P. Quentin, Nucl. Phys. **A238**, 28 (1975).
 [24] V. Baran *et al.*, Proceedings of the VI International School on Heavy Ion Physics, Dubna, 1997.
 [25] J. Bartel, P. Quentin, M. Brack, C. Guet, and H.-B. Håkansson, Nucl. Phys. **A386**, 79 (1982).
 [26] A. Bohr and B.R. Mottelson, *Nuclear Structure Vol. I* (W.A. Benjamin, New York, 1969).
 [27] P. Möller and J.R. Nix, Nucl. Phys. **A536**, 20 (1992); P. Möller, J.R. Nix, W.D. Myers, and W.J. Swiatecki, At. Data Nucl. Data Tables **59**, 185 (1995).
 [28] S. Yoshida and N. Takigawa, Phys. Rev. C **55**, 1255 (1997).
 [29] J.R. Ficenec, L.A. Fajardo, W.P. Trower, and I. Sick, Phys. Lett. **42B**, 213 (1972); J. Eberz, U. Dinger, G. Huber, H. Lochmann, R. Menges, R. Kirchner, O. Klepper, T. Köhl, and D. Marx, Z. Phys. A **326**, 121 (1987); H. de Vries, C.W. Jäger, and C. de Vries, At. Data Nucl. Data Tables **36**, 495 (1987).